J Mater Sci (2008) 43:4729–4736
DOI 10.1007/s10853-007-2351-x

REACTIVITY OF SOLIDS

A quenching apparatus for the gaseous products of the solar thermal dissociation of ZnO

D. Gstoehl · A. Brambilla · L. O. Schunk · A. Steinfeld

Received: 23 August 2007 / Accepted: 27 November 2007 / Published online: 30 April 2008

Abstract Rapid cooling for avoiding the recombination of Zn vapor and O_2 derived from the solar thermal dissociation of ZnO is investigated using a thermogravimeter coupled to a quenching apparatus. The ZnO sample, which is placed in a cavity receiver and directly exposed to concentrated solar irradiation, underwent dissociation in the temperature range 1,820–2,050 K at a rate monitored by on-line thermogravimetry. The product gases were quenched by water-cooled surfaces and by injection of cold Ar at cooling rates from 20,000 to 120,000 K/s, suppressing the formation of ZnO in the gas phase and at the walls. Zinc content of the collected particles downstream varied in the range 40–94% for Ar/Zn(g) dilutions of 170 to 1,500.

Nomenclature

b.p.	Boiling point
CR	Cooling rate, K/s
D	Dilution (n_{Ar}/n_{Zn})
d_i	Injector diameter, mm
L_{HZ}	Length of quench device inlet, mm
L_n	Liters under standard conditions at 273.15 K and 1 atm
m.p.	Melting point
$\dot{m}_{ZnO}$	ZnO dissociation rate, mg/s
n	Number of atoms, mol
$\dot{n}$	Molar flow rate, mol/s
p	Partial pressure, Pa
T	Temperature, K
$X_{particles}$	Zinc yield based on collected particles
$Y_{instantaneous}$	Zinc yield based on oxygen balance
z	Distance from quench device inlet, mm

Subscripts

AF	Annular flow
sat.	Saturation
CZ	Cold zone of quench device
dec.	Decomposition
HZ	Hot zone of quench device
QF	Quench flow
RF	Reacting flow

D. Gstoehl (✉) · A. Brambilla · L. O. Schunk · A. Steinfeld
Solar Technology Laboratory, Paul Scherrer Institute,
5232 Villigen, Switzerland
e-mail: daniel.gstoehl@psi.ch

A. Steinfeld
Department of Mechanical and Process Engineering,
ETH Zurich, 8092 Zurich, Switzerland

Introduction

The production of solar hydrogen via a two-step H_2O-splitting thermochemical cycle using ZnO/Zn redox reactions can be represented by [1]:

$$\text{1st step (solar):} \quad ZnO \rightarrow Zn + 0.5\,O_2 \tag{1}$$

$$\text{2nd step (non-solar):} \quad Zn + H_2O \rightarrow ZnO + H_2 \tag{2}$$

In the first endothermic solar step, ZnO is thermally dissociated into Zn and O_2. In the second exothermic non-solar step, Zn is steam-hydrolyzed to form H_2 and ZnO; the latter is recycled to the first step. The net reaction is $H_2O = H_2 + 0.5O_2$, but since H_2 and O_2 are formed in different steps, the need for high-temperature gas separation is thereby eliminated. This cycle has been identified as a promising path for solar hydrogen production because of its potential of reaching high energy conversion efficiencies, and consequently, the

potential of economic competitiveness [1, 2]. Several chemical aspects of the thermal dissociation of ZnO have been previously investigated [3]. The reaction is highly endothermic (ΔH_{298K} = 351 kJ/mol) and proceeds at reasonable rates at above 1,900 K. The products Zn(g) and O_2 need to be quenched or separated at high temperatures to avoid their recombination. In particular, the zinc yield is sensitive to the dilution ratio of Zn(g) in an inert gas flow and to the temperature of the surface on which the products are quenched [3, 4]. The condensation of zinc vapor in the presence of O_2 was studied by fractional crystallization in a temperature-gradient tube furnace [5]. It was found that Zn oxidation is heterogeneous in nature and, in the absence of nucleation sites, Zn(g) and O_2 can coexist in a meta-stable state. Alternative to quenching, electrothermal methods for in situ separation of Zn(g) and O_2 at high temperatures have been experimentally demonstrated to work in laboratory reactors [6]. Nevertheless, high-temperature separation of Zn vapor and O_2 remains a technological challenge. Quenching, although thermodynamically inefficient, is the preferred option because of its simplicity. Common techniques for rapid cooling a hot gas stream include—listed with increasing cooling rates—contact with a cold surface, evaporation of a liquid spray, injection in a fluidized bed, mixing with a cold gas, and expansion of a pressurized gas [7]. Zn(g)/O_2 mixtures were quenched by contact with cold walls [4, 8, 9], but Zn(s) deposition in layers of increasing thickness reduced the cooling efficiency and hindered steady-state operation. The objective of the current study is to develop and experimentally demonstrate an effective quenching apparatus for Zn(g)/O_2 mixtures exiting the solar reactor for obtaining high yield of Zn under continuous mode of operation. The design concept is aimed at minimizing surface wall exposure and the surface-to-volume ratio of zinc droplets/particles by controlling diffusion, dilution, and cooling rate.

The quench concept

The design of the quench apparatus is based on the simplified description of the zinc oxidation process illustrated in Fig. 1. Heterogeneous oxidation of Zn(g) occurs in the presence of a surface, which—in the absence of foreign particles—could be a wall, a Zn droplet or particle, or a ZnO particle. The temperature drop from the ZnO dissociation temperature to ambient temperature is divided into three regions. In the first region A, the temperature is above the decomposition temperature of ZnO, where Zn(g) oxidation is thermodynamically unfavorable. In the second region B, the temperature is below the decomposition

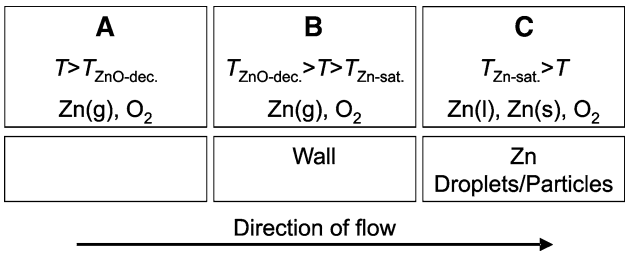

Fig. 1 Quench concept based on three temperature regions

temperature of ZnO but still above the saturation temperature of Zn, where Zn(g) and O_2 form a meta-stable gas mixture and ZnO can only be formed by reaction on the walls. In the third region C, the temperature is below the Zn saturation temperature, where Zn(g) nucleates homogeneously, forming droplets and particles that serve as preferential sites for oxidation, in addition to the walls.

To avoid Zn reoxidation occurring in the regions B and C, the quenching apparatus was designed following a three-zone approach. In the hot end of the quench unit facing the exit of the solar reactor, the wall temperature is kept close or higher than that of ZnO decomposition to suppress the formation of ZnO. Downstream, in the cold end of the quench unit, the temperature is decreased sharply to slow the oxidation kinetics. In the transitional zone between the hot and the cold ends, where ZnO is likely to be formed on the walls, an inert gas curtain is created to diminish Zn(g)/O_2 diffusion to the walls.

The quench apparatus

A scheme of the quench apparatus is depicted in Fig. 2. It features hot, transition, and cold zones that correspond to the regions A, B, and C of Fig. 1, respectively. The hot and transition zones have been realized by a set of three Al_2O_3 concentric tubes. In the hot zone, the Zn(g)/O_2 flow mixture diluted in Ar that exits the solar reactor (denoted RF: Reacting Flow) enters the quenching unit. RF's mass flow rate is set to 8 L_n/min[1]; its temperature is $T_{RF} > 1{,}800$ K. In the transition zone, the RF is surrounded by an annular Ar flow (denoted AF: Annular Flow) for suppressing diffusion of RF to the walls. Zinc droplet formation is avoided by maintaining the AF's temperature at $T_{AF} = 870$ K, about 50 K higher than the Zn saturation temperature for the given experimental conditions (see Table 1 in the next section). Mixing between RF and AF is minimized by selecting the tube diameters (i.d. = 15 mm in the hot zone and i.d. = 20 mm in the transition zone) and the AF's mass flow rate (set to 10.5 L_n/min) to keep velocities in the

[1] L_n means liters under standard conditions at 273.15 K and 1 atm.

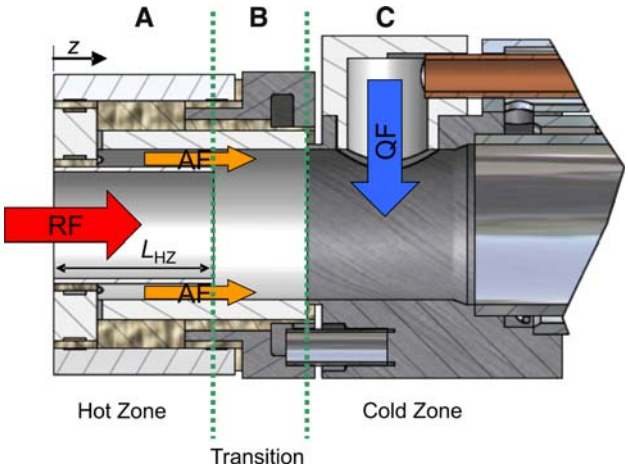

Fig. 2 Schematic of the quench apparatus illustrating the three temperature zones

laminar flow regime. The cold zone consists of a water-cooled stainless steel tube containing a port for the injection of cold Argon (denoted QF: Quench Flow). QF's temperature is $T_{QF} = 298$ K; its mass flow rate is set to 27 L_n/min to ensure that the mixture reaches a temperature below the Zn m.p. (693 K). For a single jet orthogonal to the pipe axis, efficient mixing is accomplished by centering the jet on the pipe axis at a distance of at least two pipe diameters from the injection point [10]. Applying a mixing correlation [11] for a Reynolds number of the jet lower than 9000 yields an injector's diameter $d_i = 13$ mm. A CFD parametric simulation and sensitivity analysis indicate that varying T_{RF} from 1,000 to 1,800 K results in an increase of d_i from 10 to 13 mm, and that varying T_{AF} from 500 to 1,000 K results in an increase of d_i from 12 to 14 mm. For $d_i > 11$ mm, the jet stays attached to the pipe wall next to the injection point because its momentum is not enough to penetrate the core of the pipe flow. In contrast, for $d_i < 11$ mm, the jet impacts against the opposite side and stays attached to the wall or develops into an annular flow. This situation is undesired because of the difficulty to cool the hot core. Thus, $d_i = 11$ mm was selected. After injection of the quench gas, the exhaust gas tube is water-cooled over a length of 0.4 m. The temperature of the solidified zinc particles is thus further decreased by convection heat transfer—(if they remain as aerosol in the gas stream) or by conduction heat transfer—(if they deposit on the wall).

Fluid flow and heat transfer numerical simulations were performed with the CFD code Ansys CFX-10.0 by applying the shear stress transport turbulence model. The boundary temperatures of the two ceramic tubes were assumed to vary linearly from 1,900 to 1,600 K and 1,500 to 900 K, respectively, while the temperature of the water-cooled metallic tubes was set to 300 K. The computed temperature field for the design operating conditions is shown in Fig. 3. T_{RF} is maintained above 1,400 K until it reaches the position of QF injection where it decreases sharply. The cooling rates from 1,180 K (Zn b.p.) to 693 K (Zn m.p.) were calculated and averaged for 37 streamlines with starting points equally distributed over the inlet cross

Table 1 Experimental operating conditions and results

Run#	L_{HZ} (mm)	RF (L_n/min)	AF (L_n/min)	QF (L_n/min)	CR (K/s)	T_{cavity} (K)	$\dot{m}_{ZnO}$ (mg/s)	D_{HZ}	D_{CZ}	$p_{Zn,HZ}$ (Pa)	$p_{Zn,CZ}$ (Pa)	$X_{particles}$ (mol%)
1	24	8	10.5	27	77,000	1,831	1.8	265	1,510	380	67	85
2	24	8	10.5	27	77,000	1,821	2.9	167	948	603	107	89
3	24	8	10.5	27	77,000	1,827	3.3	147	835	683	121	90
4	24	8	5	27	116,000	1,840	4.6	107	534	936	189	94
5[a]	24	8	10.5	27	77,000	1,829	5.8	83	473	1,198	213	83
6	24	8	10.5	27	77,000	1,976	15.3	32	181	3,035	554	50
7[a]	12	8	10.5	27	77,000	1,843	2.2	224	1,273	450	79	85
8	12	8	10.5	27	77,000	1,925	2.7	179	1,017	562	99	75
9	12	5.3	7	18	64,000	1,877	2.4	134	765	747	132	61
10	12	8	2	27	46,000	1878	3.2	152	705	658	143	58
11	12	8	10.5	27	77,000	1,845	5.6	87	495	1,143	204	73
12	12	5.3	3.5	18	88,000	1,919	3.7	88	445	1,130	227	82
13	12	5.3	7	9	18,000	1,916	4.7	68	275	1,449	367	40
14	12	8	10.5	27	77,000	1,989	11.1	44	250	2,228	402	70
15	12	5.3	7	27	117,000	2,050	9.9	32	240	2,982	419	76
16	12	5.3	3.5	18	88,000	2,025	9.8	33	166	2,940	604	60

[a] AF preheated to 970 K

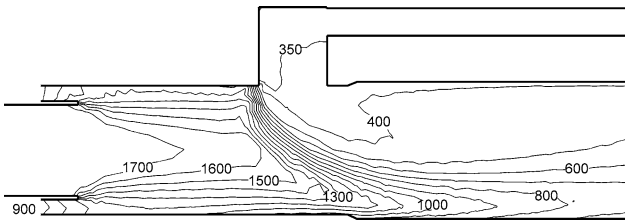

Fig. 3 Computed temperature contour map at design operating conditions (temperatures in K)

section of the quench unit. For the design operating condition, a mean cooling rate of 77,000 K/s was predicted.

The solar thermogravimeter reactor

A schematic of the solar thermogravimeter reactor is shown in Fig. 4. It consists of solar cavity receiver, i.e. a well-insulated enclosure (i.d.: 152 mm, length: 150 mm), made of CaO-stabilized ZrO_2 bricks (thickness: 50 mm) over two layers of porous Al_2O_3 (thickness 36 mm each), that contains a 60-mm-diameter circular opening—the *aperture*—to let in concentrated solar radiation through a transparent 3-mm-thick quartz window. Inside the cavity, the ZnO sample is mounted on an Al_2O_3 rod that is suspended on a balance (Mettler Toledo; accuracy: 0.01 g). With this arrangement, the ZnO sample is directly exposed to concentrated solar irradiation, while its weight loss during dissociation is monitored continuously. The sample consists of pressed and sintered ZnO tile of thickness

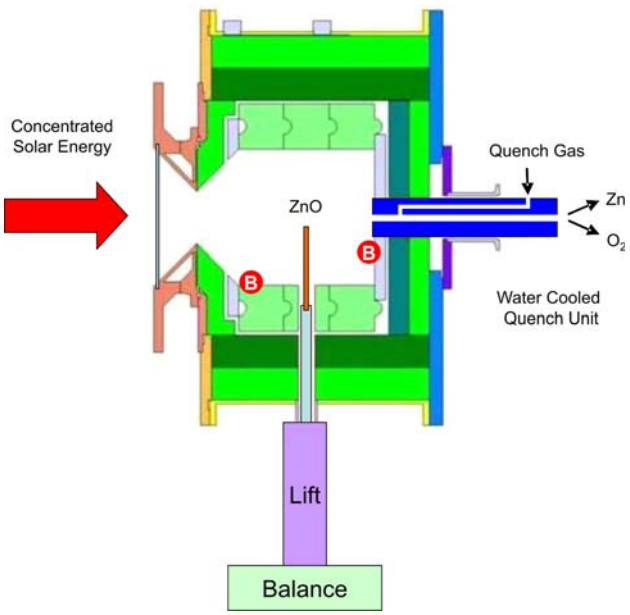

Fig. 4 Schematic of the experimental set-up with the solar thermogravimeter and the quench apparatus

2.5 mm, width 18 mm, and length 120 mm. This setup allows retracting the ZnO tile into the insulation to avoid premature dissociation during preheating of the cavity. At the beginning of an experimental run, the ZnO tile is located inside the insulation. The reactor is then heated to the desired temperature and maintained under isothermal conditions before the ZnO sample is lifted up to 40 mm into the hot cavity. The source of energy is concentrated thermal radiation from PSI's High-Flux Solar Simulator (HFSS): an array of ten 15 kW_e high-pressure xenon arcs, each closed-coupled with truncated ellipsoidal specular reflectors of common focus [12]. This research facility reaches solar concentration ratios exceeding 11,000 suns (1 sun = 1 kW/m^2) and closely approximates the heat transfer characteristics of highly concentrating solar systems, such as solar towers and solar furnaces. The nominal cavity temperature, denoted T_{cavity}, is determined by the arithmetic mean value of two shielded thermocouples type-B located in the front and rear of the cavity, as indicated in Fig. 4. The window is aerodynamically protected from condensation of Zn vapor by injecting Ar at the window and aperture planes. In addition, Ar is introduced in the box containing the balance for preventing back-flow of hot gases. The Ar flow rates were set 2.3 to 3 L_n/min at the window, 0 to 1 L_n/min at the aperture, and 2.3 to 4 L_n/min at the balance. This inert gas flow helps carry the product gases of the ZnO dissociation into the outlet port at the rear of the cavity. The cavity pressure is measured behind the quartz window. Typical operating values are about 60 mbar above atmospheric pressure. The maximum allowed pressure in the cavity is set to 150 mbar by a safety valve. Gas flow rates are controlled with electronic flow controllers (Bronkhorst). Data are acquired with a sampling frequency of 1 Hz. The product gases of the ZnO dissociation, diluted in Ar, exit the cavity and enter the quench apparatus described in Sections "The Quench Concept" and "The Quench Apparatus".

Particles formed are collected downstream in a glass microfiber filter with pore size of 2.7 μm and analyzed after termination of each experiment by X-ray diffraction (XRD, Philips Xpert, FeK α, $\lambda = 1.93740$ Å). The composition of the product gases is analyzed by gas chromatography (Agilent High Speed Micro GC G2890A, equipped with molecular sieve 5A and HaySep A capillary columns), by IR-based detectors for CO and CO_2 (Siemens Ultramat 23), and by thermal conductivity-based detector for O_2 (Siemens Oxymat 6). The GC has a 10-ppm detection limit at a low sampling rate of 0.33 min^{-1}. The IR detector has detection limits of 0.2% for CO and CO_2, at a sampling rate of 1 s^{-1}. The conductivity-based detector has a detection limit of 50 ppm at a sampling rate of 1 s^{-1}. The presence of CO and CO_2 is monitored to ensure that ZnO was not reduced carbothermally.

The instantaneous zinc yield is defined as:

$$Y_{\text{instantaneous}} = \frac{2 \cdot \dot{n}_{O_2}}{\dot{n}_{ZnO}} \tag{3}$$

where $\dot{n}_{O_2}$ is the molar flow rate of O_2, measured on-line at the outlet gas; and $\dot{n}_{ZnO}$ is the molar flow rate of ZnO dissociated, measured on-line as the rate of weight loss recorded by the balance. After each experimental run, products collected from the filter and from deposits in the quench unit are analyzed for their Zn and ZnO content by XRD, with an accuracy of 7%. The zinc yield is defined as the Zn content of particles collected downstream of QF injection,

$$X_{\text{particles}} = \left(\frac{n_{Zn}}{n_{Zn} + n_{ZnO}} \right)_{\text{collectedparticles}} \tag{4}$$

Error analysis was determined by sequential perturbation and then combined using the root sum square method [13]. The dominating contribution to the uncertainty of the zinc yield derives from the uncertainty of the XRD analysis, resulting in an absolute error of ±7%. The dilution of Zn(g) in Ar has been calculated for two extremes. The lower limit is obtained at the inlet of the quench unit in the hot zone (HZ):

$$D_{HZ} = \frac{n_{\text{Ar in RF}}}{n_{Zn}} = \frac{n_{\text{Ar in RF}}}{n_{ZnO,\text{dissociated}}} \tag{6}$$

where $n_{\text{Ar in RF}}$ is the total number of moles of Ar in RF integrated over the duration of the experimental run. The upper limit of dilution is obtained after the quench unit in the cold zone (CZ):

$$D_{CZ} = \frac{n_{\text{Ar in RF+AF+QF}}}{n_{Zn}} = \frac{n_{\text{Ar in RF+AF+QF}}}{n_{ZnO,\text{dissociated}}} \tag{7}$$

The zinc partial pressures are defined in analogy to the dilution, namely

$$p_{Zn,HZ} = p_0 \frac{n_{Zn}}{n_{\text{Ar in RF}} + n_{Zn} + n_{O_2}} = p_0 \frac{n_{ZnO,\text{dissoicated}}}{n_{\text{Ar in RF}} + 1.5 \cdot n_{ZnO,\text{dissociated}}} \tag{8}$$

$$p_{Zn,CZ} = p_0 \frac{n_{ZnO,\text{dissoicated}}}{n_{\text{Ar in RF+AF+QF}} + 1.5 \cdot n_{ZnO,\text{dissociated}}} \tag{9}$$

where p_0 is the atmospheric pressure.

Experimental results

Sixteen solar experimental runs were performed for cavity temperatures in the range 1,821–2,050 K. Two geometrical configurations for the hot zone were examined: the length of the innermost ceramic tube was either 24 mm as shown in Fig. 2 or shortened to 12 mm. Their operational conditions and results are listed in Table 1, sorted by increasing partial pressure $p_{Zn,CZ}$. About 3 g ZnO was dissociated in every run. The dissociation rate $\dot{m}_{ZnO}$ was in the range 1.8–15.3 mg/s, which results in molar Ar/Zn dilutions for the hot and cold zones in the range of 30–270 and 170–1500, respectively. $p_{Zn,HZ}$ varied in the range 380–3,035 Pa, while $p_{Zn,CZ}$ varied in the range 67–604 Pa, as a result of the injection of AF + QF. In runs #5 and #7 an electrical heater was used to preheat AF to 970 K.

The gas temperature distribution along the centerline of the quench apparatus was measured by a set of type-K thermocouples of diameters 0.5, 1, and 1.5 mm that were positioned at distances ranging from 10 to 80 mm from the inlet of the quench unit. The extrapolation method to zero diameter was applied to compensate for errors due to conduction and radiation heat transfer [14]. Figure 5 shows the measured gas temperature profiles for two selected mass flow rates of QF: 9 L_n/min for run #13 and 27 L_n/min for run #15 (see Table 1). In the hot and transition zones, the temperature was generally maintained above 1,300 K. At a distance of 42 mm from the inlet, it dropped sharply to about 500 K as a result of the QF injection, to finally attain 700 K in the cold zone. As expected, for the lower QF of 9 L_n/min, the temperature decrease was less pronounced.

The gas temperature distributions predicted by CFD are also shown in Fig. 5. The calculated profiles reach somewhat higher values in the hot zone while the temperature drop is shifted to the right, attributed to the boundary condition assumed. However, their slope is in good agreement with the corresponding measured ones. The cooling rates, derived from the calculated slopes of the temperature profiles along flow streamlines, were 18,000 and 117,000 K/s for runs #13 and #15, respectively. The cooling rates along flow streamlines, which are lower than those along the centerline of the quench apparatus but better represent the cooling process of particles in the flow field, are listed for all runs in Table 1.

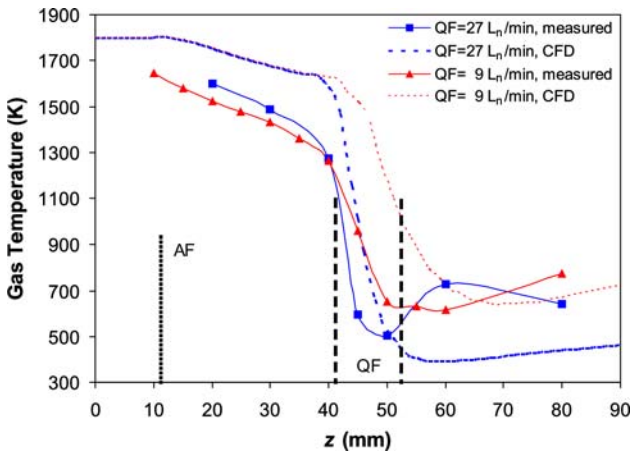

Fig. 5 Temperature profiles measured (runs #13 and #15 in Table 1) and computed (by CFD) along the centerline of the quench apparatus

A representative experimental run (run #5 in Table 1) is shown in Fig. 6. Isothermal conditions were reached after a heating period of 2 h. Dissociation started immediately once the ZnO sample is lifted into the hot cavity and exposed to the direct high-flux irradiation, as indicated by the weight loss monitored by the balance and by the O_2 measured in the off-gas. Initially, the dissociation increased sharply, reached 8 mg/s, and afterward achieved steady state at 6 mg/s. The maximum O_2 concentration was observed about 30 s after the peak in the dissociation rate because of the time lag of the gas analysis. About 40 ppm of background O_2 from leaked air was present before and after the run, which was subtracted from the product O_2. $Y_{instantaneous}$ reached 30% and decreased to 20%. At the end of the experimental run, there was still some remaining oxygen in the cavity leading to an artificial increase of $Y_{instantaneous}$ due to its definition by Eq. 3.

After each experimental run, the quench apparatus was examined for deposits. At a distance of 9 to 12 mm from the inlet, ZnO needles were found as shown in Fig. 7. The run number, the cavity temperature T_{cavity}, and the length of the innermost ceramic tube in the hot zone L_{HZ} are indicated. In some selected runs, e.g. run #2, the extent of deposition covered the whole cross section. However, this needle meshwork was still permeable, resulting in a small pressure drop. The beginning of the deposits was shifted in the flow direction at higher cavity's temperatures. For the runs with the shorter tube (L_{HZ} = 12 mm), less ZnO needles were formed because of the higher wall temperatures reached by radiation emitted from the hot cavity. Fewer

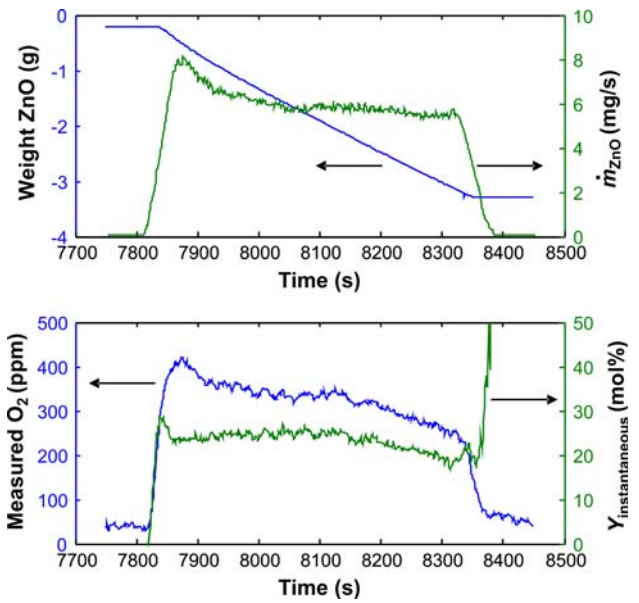

Fig. 6 Weight loss due to ZnO dissociation and dissociation rate (top), and measured oxygen in the off-gas and instantaneous zinc yield (bottom), as a function of time obtained during a representative experimental run at PSI's High-Flux Solar Simulator

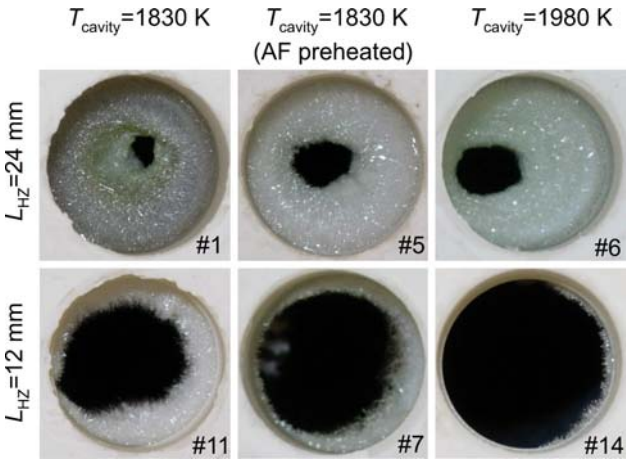

Fig. 7 Front view of ZnO deposition at the inlet region (HZ) of the quench apparatus

deposits were also observed for the two runs with the preheated annular gas flow (AF), runs #5 and #7. For example, the amount of ZnO deposited in the hot zone was 35 mg in run #7, as compared to 330 mg in run #1 (see Fig. 7). Practically, no deposition occurred in the transition zone, demonstrating that the wall protection by the annular flow worked well and succeeded to eliminate diffusion of Zn/O_2 toward the wall. The amount of deposits in the hot zone ranged from 1 to 30% of the total amount of dissociated ZnO. The total mass of deposits collected in the quench tube and on the filter varied from 0.2 to 1.2 g and from 0.6 to 1.4 g, respectively, which together represent 40 to 70% of the total molar amount of dissociated ZnO. The rest was left inside the cavity and could not be recovered.

Scanning electron microscope (SEM) photographs of the reactants and of deposits in the filter are displayed in Fig. 8. The grain size of the pressed and sintered ZnO used as reactants was 2–10 μm. The deposits collected in the filter are considerably smaller and result from dissociation/condensation/reoxidation processes. They exhibit round and prismatic particles of 100–200 nm size, similar to those observed previously in a temperature-gradient tube furnace [5]. Presumably, the round particles were obtained from homogeneous nucleation of Zn with subsequent solidification of zinc droplets, while the prismatic-shaped particles were obtained by direct transition from the gas to the solid phase.

$X_{particles}$ was in the range 40–94%, with 3–70% for particles collected in the quench apparatus and 54–100% for particles collected in the filter. In general, $X_{particles}$ was higher for the fraction recovered in the filter than that on the walls of the quenching zone, as observed previously [4]. Figure 9 shows $X_{particles}$ as a function of $p_{Zn,CZ}$. The vertical dashed line indicates $p_{Zn,CZ}$ corresponding to the triple point (22 Pa), below which Zn(g) can be condensed

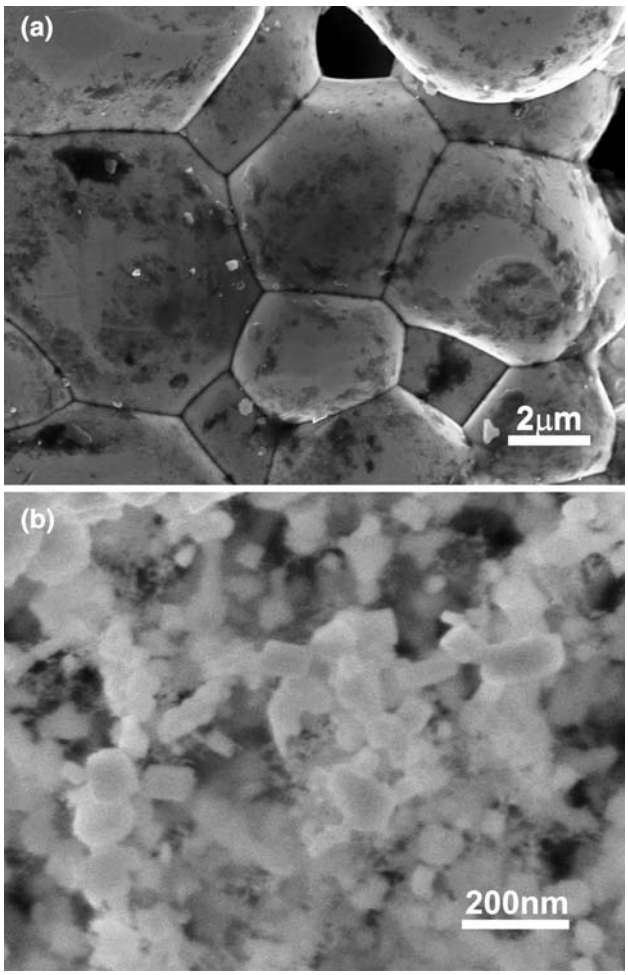

Fig. 8 SEM photographs of (**a**) ZnO reactants, and (**b**) solid products collected on filter (run #6)

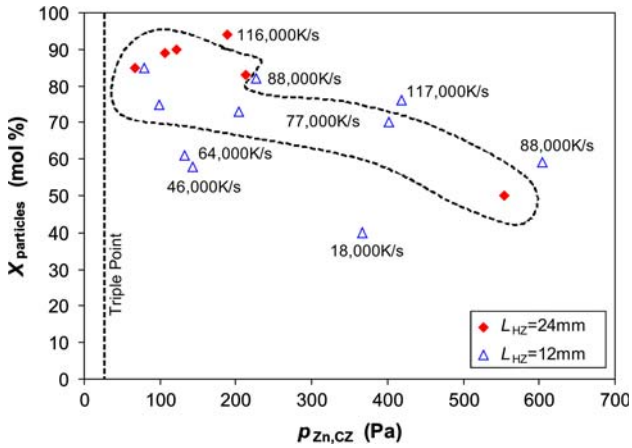

Fig. 9 Zinc yield of products collected after the quench versus zinc partial pressure in the cold zone (CZ) for both geometrical configurations. Labels indicate cooling rates

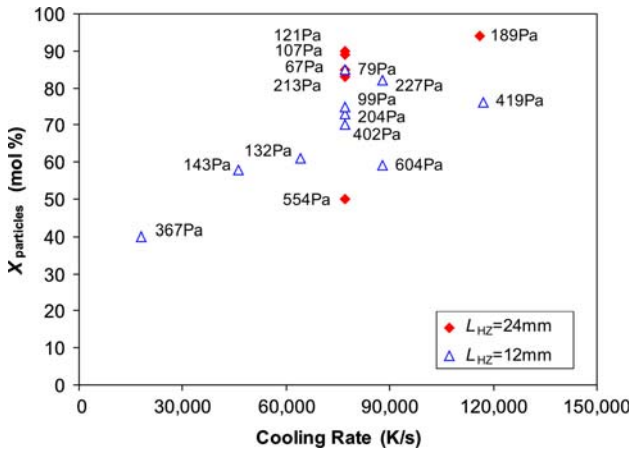

Fig. 10 Zinc yield of products collected after the quench versus cooling rate derived from CFD simulations for both geometrical configurations. Labels indicate zinc partial pressures in the cold zone ($p_{Zn,CZ}$)

without passing through a liquid phase. The zinc yield was in the range 58–94% for $p_{Zn,CZ} < 200$ Pa and decreased to 40–76% for higher zinc partial pressures. The estimated cooling rate evaluated along streamlines is indicated next to each data point. Those obtained at the design operating conditions with a cooling rate of 77,000 K/s are enclosed by the dashed curve. Figure 10 is a cross plot of Fig. 9 and shows $X_{particles}$ as a function of the cooling rate; this time $p_{Zn,CZ}$ is indicated next to each data point. In general, high zinc yields were obtained at high cooling rates and low $p_{Zn,CZ}$.

Summary and conclusions

A quenching apparatus was designed and fabricated for avoiding the recombination of gaseous products Zn(g) and O_2 derived from the solar thermal dissociation of ZnO. It features three zones: (1) an inlet hot zone, where the wall temperature is kept close or above the ZnO decomposition temperature; (2) a transition zone at above the Zn saturation temperature where an annular Ar flow avoids Zn(g)/O_2 reaction at the walls; and (3) an outlet cold zone with water-cooled walls and injection of Ar quench gas. Experimentation was performed using a solar thermogravimeter in which samples of ZnO were directly exposed to concentrated solar radiation while their rate of dissociation was monitored on-line. The exit of the solar thermogravimeter was integrated to the inlet of the quench apparatus. The annular flow protection worked well and eliminated deposits in the transition zone. Zinc yields of up to 94% were obtained when using Ar/Zn dilution of 530 and a cooling rate of about 10^5 K/s. Results indicate the technical feasibility of avoiding Zn/O_2 recombination by quenching the gas products in a continuous solar process.

Acknowledgments Funding by the Swiss Federal Office of Energy is gratefully acknowledged. We thank S. Wepf, L. Donati, and K. Cuche for technical help at PSI's High-Flux Solar Simulator; E. Guglielmini and H. Fries for the CFD simulations; A. Weber for the SEM photographs; A. Frei for the XRD analysis; and D. Colzani and Ch. Wieckert for fruitful discussions.

References

1. Steinfeld A, Palumbo R (2001) In: Meyers RA (ed) Encyclopedia of physical science & technology 15. Academic Press, p 237
2. Perkins C, Weimer AW (2004) Int J Hydrogen Energy 29:1587
3. Palumbo R, Lédé J, Boutin O, Elorza-Ricart E, Steinfeld A, Moeller S, Weidenkaff A, Fletcher EA, Bielicki J (1998) Chem Eng Sci 53(14):2503
4. Lédé J, Elorza-Ricart E, Ferrer M (2001) J Sol Energy Eng 123:91
5. Weidenkaff A, Steinfeld A, Wokaun A, Auer PO, Eichler B, Reller A (1999) Sol Energy 65(1):59
6. Fletcher EA (1999) Ind Eng Chem Res 38:2275
7. Sundstrom DW, Demichiell RL (1971) Ind Eng Chem Process Des Develop 10(1):114
8. Ferrer M, Lédé J (1999) Sol Energy 66(2):151
9. Elorza-Ricart E (2002) Genie des procedes thermochimiques solaires. Application a la dissociation thermique, suivie de trempe, de l'oxyde de zinc. PhD, Institut National Polytechnique de Lorraine
10. Forney LJ (1986) In: Cheremisinoff PN (ed) Encyclopedia of fluid mechanics 2. Gulf Publishing Company, Houston, p 660
11. Forney LJ, Lee HC (1982) AIChE J 28(6):980
12. Petrasch J, Coray P, Meier A, Brack M, Haeberling P, Wuillemin D, Steinfeld A (2007) J Sol Energy Eng 129(4):405
13. Moffat RJ (1985) J Fluids Eng 107:173
14. Michalski L, Eckersdorf K, Kurcharski J, McGhee J (2001) Temperature measurement. John Wiley & Sons Ltd, p 369